HAL
open science

Thermal activation effects on the exchange bias in ferromagnetic-antiferromagnetic nanostructures

Vincent Baltz, J. Sort, B. Rodmacq, B. Dieny, S. Landis

To cite this version:

Vincent Baltz, J. Sort, B. Rodmacq, B. Dieny, S. Landis. Thermal activation effects on the exchange bias in ferromagnetic-antiferromagnetic nanostructures. Physical Review B: Condensed Matter and Materials Physics (1998-2015), 2005, 72, pp.104419. 10.1103/PhysRevB.72.104419 . hal-01683704

HAL Id: hal-01683704

https://hal.science/hal-01683704

Submitted on 25 May 2019

HAL is a multi-disciplinary open access archive for the deposit and dissemination of scientific research documents, whether they are published or not. The documents may come from teaching and research institutions in France or abroad, or from public or private research centers.

L'archive ouverte pluridisciplinaire **HAL**, est destinée au dépôt et à la diffusion de documents scientifiques de niveau recherche, publiés ou non, émanant des établissements d'enseignement et de recherche français ou étrangers, des laboratoires publics ou privés.

Thermal activation effects on the exchange bias in ferromagnetic-antiferromagnetic nanostructures

V. Baltz,* J. Sort, B. Rodmacq, and B. Dieny
SPINTEC (URA 2512), CEA/CNRS, 17 Avenue des Martyrs, 38054 Grenoble Cedex 9, France

S. Landis
LETI/D2NT, CEA, 17 Avenue des Martyrs, 38054 Grenoble Cedex 9, France
(Received 20 April 2005; revised manuscript received 8 July 2005; published 9 September 2005)

The hysteresis loop shift H_E of sub-100-nm ferromagnetic- (FM-) antiferromagnetic (AFM) nanostructures is found to be strongly influenced by thermal activation effects. These effects, which tend to reduce H_E, are more pronounced in the nanostructures than in continuous films with the same composition, particularly for thin AFM layers. In addition, the reduced dimensions of the nanostructures also impose spatial constraints to the AFM domain size, particularly for thick AFM layers. This favors an enhancement of H_E. Due to the interplay between these two competing effects, the loop shift in the dots can be either larger or smaller than in the continuous films with the same composition, depending on both the AFM thickness and temperature. A temperature-AFM thickness phase diagram, separating the conditions resulting in larger or smaller H_E in the nanostructures with respect to continuous film is derived.

DOI: 10.1103/PhysRevB.72.104419 PACS number(s): 75.75.+a, 75.60.−d

I. INTRODUCTION

The exchange interactions between ferromagnetic (FM) and antiferromagnetic (AFM) materials typically result in a shift of the hysteresis loop, along the magnetic field axis (H_E), referred to as exchange bias (EB), which is usually accompanied with an enhancement of the coercivity (H_C).[1] These effects are often ascribed to the formation of AFM domains which result in AFM uncompensated interfacial spins. During magnetization reversal, strongly pinned AFM uncompensated spins give rise to the loop shift, whereas unpinned spins are mainly responsible for the coercivity enhancement.[2–5] Upon heating, a decrease of H_E is observed since the anisotropy and exchange energies in the AFM have to compete with thermal energy, which tends to reduce the stability of the AFM spin lattice and, consequently, the pinning strength that the AFM exerts on the FM. The temperature at which the exchange bias completely disappears is called the blocking temperature (T_B) and is below the Néel temperature of the AFM (particularly for thin AFM).

During the last decades, a large variety of applications such as magnetoresistive read heads or magnetic random access memories (MRAMs) have triggered the study of EB properties.[6] The constant miniaturization of devices[7] has recently motivated studies of EB properties in systems with reduced lateral dimensions.[8–24] Such investigation of confined EB systems down to length scales comparable to the AFM domains sizes is crucial for a better understanding of the EB phenomenon, since it allows probing the role of AFM domains on EB. However, the effects of confinement, such as the alteration of the AFM domain structure in nanostructures, have been far less explored. In particular, EB was investigated in nanostructures whose lateral sizes were varied, while keeping the AFM thickness constant (i.e., two-dimensional confinement of the AFM).[8,10–12,15,16,18] Occasionally, the effects of the temperature on the EB properties of nanostructures have also been reported.[9,11,12] It is noteworthy that some of the results from different groups seem contradictory. Namely, although in some systems H_E is found to increase in the nanostructures with respect to the continuous film,[8–11] the opposite behavior is encountered in other systems.[12–22] We have recently shown that, at room temperature, for a given dot size, either an enhancement or a reduction of H_E can be obtained in the FM-AFM dots, depending on the AFM thickness.[23] Thermal activation is found to play a crucial role on this effect. Many experimental[25–32] and theoretical[30–35] studies have been performed on continuous films to better understand thermal activation effects (e.g., after effects, blocking temperature distributions, …) on the EB properties. Surprisingly, although thermal activation plays a role in EB properties, few systematic studies on these effects have been carried out in nanostructures.[11,12]

In this article, we report on thermal activation effects on the EB of sub-100-nm FM-AFM bilayers sputtered on prepatterned Si/SiO_2 square dots. We demonstrate that systems with nanostructured and/or thinner AFM layers are more prone to thermal activation effects than continuous and/or thicker AFM layers. From the interplay between thermal activation effects (which reduce H_E) and the physically imposed spatial constraints on the AFM domain size (which can induce an enhancement of H_E), we show that the magnitude of the hysteresis loop shift H_E in the nanostructures can be either larger or smaller than in continuous films with the same composition, depending on both the AFM thickness and temperature conditions.

II. EXPERIMENT

The nanostructures were fabricated by first patterning thermally oxidized Si wafers by electron beam lithography and reactive ion etching to form arrays of Si/SiO_2 square dots, with lateral sizes of 90 nm, height of 300 nm, and periodicity of 200 nm, as shown in Fig. 1. A series of samples consisting of stacks of

 ©2005 The American Physical Society

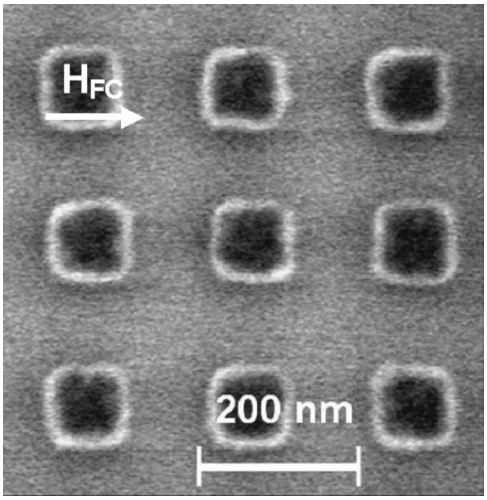

FIG. 1. Scanning electron microscopy (SEM) image of the array of 90×90 nm^2 square dots fabricated by first patterning a Si/SiO_2 wafer and subsequently depositing the FM-AFM bilayer structure.

Ta(5 nm)/Py(12 nm)/IrMn(t_{IrMn})/Pt(2 nm) (where Py denotes permalloy, i.e., $Ni_{81}Fe_{19}$, which is FM and IrMn stands for $Ir_{20}Mn_{80}$, which is AFM) were simultaneously dc sputtered, on continuous and patterned Si/SiO_2 wafers. The Ta and Pt are, respectively, buffer and capping layers. All depositions were performed at room temperature under a 2.5 Pa Ar pressure with deposition rates around 0.08 nm s^{-1}.[36] The IrMn thickness t_{IrMn} was varied from 5 to 19 nm. It should be noted that the direct deposition of the magnetic material on the already prepatterned substrates allows avoiding possible degradation effects due to post-deposition etching, such as partial structural deterioration of the layers.[36,37]

The EB was set by post annealing and field cooling the samples in a 5×10^{-3} Pa vacuum, from $T=550$ K (i.e., from above the blocking temperature T_B of all systems[23]) in a 2.4 kOe in-plane magnetic field, applied parallel to one of the sides of the square dots, as indicated in Fig. 1. Hysteresis loops were recorded at room temperature by longitudinal magneto-optical Kerr effect (MOKE) with a field sweep rate of about 1 Oe s^{-1} and at low temperatures by SQUID magnetometry with a lower field sweep rate around 0.03 Oe s^{-1}. The MOKE and SQUID data are both obtained by a single hysteresis loop (i.e., without averaging loops). Virtually no training effect was observed except a slight 15% loss in the magnitude of H_E for the nanostructures with $t_{IrMn}=5$ nm between the first and second loops. Care was taken for the 5-nm IrMn thick nanostructures, where the second loops were plotted and used. It should be noted that the pronounced shadowing effects resulting from the combination of the pillars height to lateral spacing ratio (300/110), together with the low incidence angle (30°) used for the Kerr measurements, allow masking the signal from the trenches when performing hysteresis loops using MOKE. However, both the signal from the dots and from the trenches are simultaneously detected when using SQUID.

Thermal activation at high temperatures was studied by applying a commonly used procedure,[30] which consists in (i) field cooling the samples under a positive field, $H_{FC}=2.4$ kOe from above T_B ($T_{heat1}=550$ K), (ii) heating the samples again but now to a lower temperature ($T_{heat2}<T_B$) and field cooling them to room temperature, using a negative field, $H_{FC}=-2.4$ kOe, (iii) measuring the hysteresis loop after the two consecutive field cooling procedures at room temperature. It is noteworthy that all the heating and cooling processes were performed under a 5×10^{-3} Pa vacuum. This procedure allows probing high temperature thermal activation effects.[30] Namely, at $T=T_{heat2}$, if thermal activation effects are present, the initially induced exchange bias (i.e., with the first cooling in positive field) will be reduced due to partial loss of the AFM pinning strength. Indeed, due to local inhomogeneities in the FM-AFM interface (roughness, defects, …) or variations in the AFM crystallite sizes, a distribution of local blocking temperatures in FM-AFM systems is typically encountered.[1] Since the samples are cooled again using a negative field, the AFM spins affected by the thermal activation at T_{heat2} will then be realigned but in the opposite direction, leading to an overall reduction of H_E when measured at room temperature after the two consecutive cooling procedures. Hence, it is possible to extract information about the thermal activation effects occurring at $T=T_{heat2}$ from the measurement at room temperature of the hysteresis loop after the two consecutive cooling procedures.

III. RESULTS AND DISCUSSION

Figure 2 shows hysteresis loops performed by MOKE, at room temperature, along the field cooling direction of (a) the continuous films and (b) the nanostructures, with compositions Ta(5 nm)/Py(12 nm)/IrMn(5 nm)/Pt(2 nm), after field cooling from different temperatures ($T_{heat2}=298$, 328, and 343 K). It can be observed that the value of H_E progressively decreases with T_{heat2} both in the continuous film and in the nanostructures. This is due to the enhanced thermal acti-

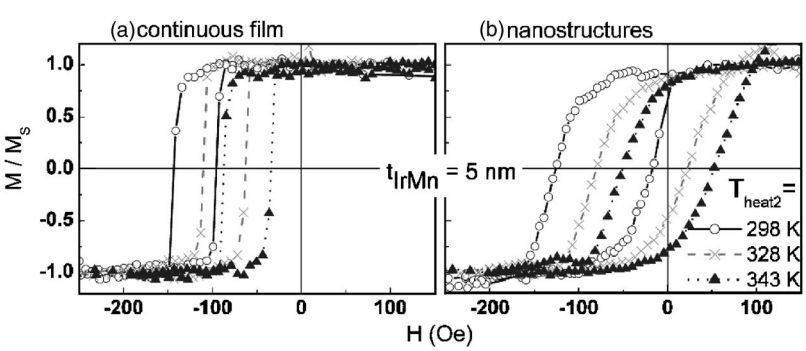

FIG. 2. Hysteresis loops of (a) the continuous films and (b) the nanostructures, with compositions Ta(5 nm)/Py(12 nm)/IrMn(5 nm)/Pt(2 nm), for different temperatures [$T_{heat2}=298$ K (-○-), 328 K (-x-), and 343 K (-▲-)] from which the continuous film and the nanostructures, previously field cooled in $H_{FC}=2.4$ kOe from above T_B, have been field cooled again in $H_{FC}=-2.4$ kOe. All measurements have been performed at room temperature by longitudinal Kerr effect along the field cooling direction.

vation at higher temperatures. Namely, if the AFM layer is sufficiently thin (e.g., 5 nm) an increasing proportion of the AFM spin lattice becomes unpinned when the temperature is raised to T_{heat2} (AFM spins which become pinned again during the second field cooling in the direction opposite to that initially set during the first field cooling).[30] Contrary to H_E, the coercivity seems to be independent on T_{heat2} for both the continuous films and the nanostructures. It is noteworthy that H_C of the dots is larger than in the continuous films ($H_{C,\mathrm{dots}} \sim 55$ Oe and $H_{C,\mathrm{cont}} \sim 30$ Oe). This trend is often encountered when comparing continuous films and nanostructures with the same composition (even without the presence of the AFM) and is mainly ascribed to the reduced number of nucleation centers and to enhanced pinning of domain walls at the edges of the nanostructures.[37,38] Additional loss in the domain wall motion is expected in FM-AFM EB unpatterned and patterned bilayers.[1,39] In unpatterned EB systems losses due to FM domain wall motion can significantly contribute to the coercivity, particularly at temperatures well below the blocking temperature. As will be further discussed, possible changes in the magnetostatic energy of the FM in EB nanostructures might account for enhanced coercivity with respect to the continuous film.[40] Moreover, in EB bilayers more pronounced dragging of the AFM spins in the nanostructures can account for an additional coercivity enhancement.[1,12,14] It is noteworthy that although the cooling procedure allows probing high temperature activation effects on H_E, thermal effects on H_C cannot be probed by using this particular heating procedure, i.e., after field cooling the system twice, using fields of opposite sign.[30] Indeed, H_C is related to AFM spins which are dragged during the magnetization reversal of the FM layer.[5] During the heating to T_{heat2}, the pinning strength exerted by the AFM spins is altered. However, once back to room temperature, this pinning recovers its initial strength. As a result, H_C remains independent of the heating temperature T_{heat2}. Furthermore, Fig. 2 reveals that for $T_{\mathrm{heat2}}=343$ K, H_E in the nanostructures has almost vanished although H_E in the continuous film is still rather large ($H_{E,\mathrm{cont}} \sim 60$ Oe). This indicates that thermal activation effects at this temperature are much larger in the nanostructures than in the continuous films. It is also noteworthy that the loops corresponding to the nanostructures are somewhat more slanted than those corresponding to the continuous films. This loop shearing is ascribed to shape inhomogeneities among the dots, which typically result in a broadening of the switching field distribution.[36] Compared to other studies of EB in patterned elements,[9,19,20] no pronounced asymmetries are observed in our case.

Figure 3(a) shows the evolution of H_E, estimated from the hysteresis loops measured at room temperature, on T_{heat2}, for both the continuous films and the nanostructures with composition Ta(5 nm)/Py(12 nm)/IrMn(t_{IrMn})/Pt(2 nm), with $t_{\mathrm{IrMn}}=5$, 9, and 16 nm. As already discussed, for a given composition the magnitude of H_E, measured at room temperature, progressively decreases with T_{heat2} and then changes sign since locally, regions of AFM spins with T_B smaller than T_{heat2} progressively reverse direction during the second field cooling procedure. It is noteworthy that, for any given t_{IrMn}, H_E in the nanostructures tends to decrease faster with T_{heat2} than H_E in the continuous films, thus evidencing

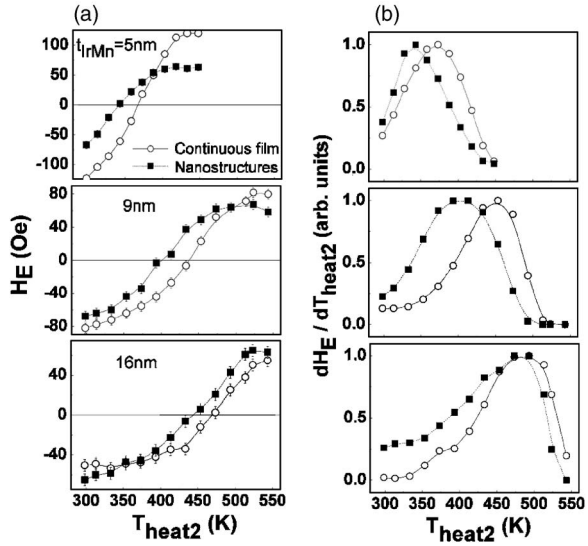

FIG. 3. (a) Dependence of the exchange bias field H_E on the temperature T_{heat2} from which the continuous film (-○-) and the nanostructures (-■-), with compositions Ta(5 nm)/Py(12 nm)/IrMn(t_{IrMn})/Pt(2 nm), with $t_{\mathrm{IrMn}}=5$, 9, and 16 nm, initially field cooled in $H_{\mathrm{FC}}=2.4$ kOe from above T_B, have been field cooled in $H_{\mathrm{FC}}=-2.4$ kOe. (b) Derivative dH_E/dT_{heat2}, of the curves plotted in (a), which are typically representative of the blocking temperature distributions. The lines are guides to the eye.

that H_E in the nanostructures is more subject to thermal activation. Moreover, H_E in the nanostructures is found to vanish at lower temperatures ($T_{HE=0}$) than in the continuous film. This means that the configuration where half of the AFM pinned uncompensated spins are oriented in one set direction and half in the opposite (i.e., where half of the regions have local blocking temperatures above $T_{HE=0}$ and half below) is observed at lower temperatures for the nanostructures. The heating temperature at which H_E levels off after the second field cooling in a negative field [see Fig. 3(a)], represents the maximum local blocking temperature and is also found to be lower in the nanostructures. Moreover, the already reported T_B reduction and/or H_C enhancement in FM-AFM nanostructures[8,9,12–15,23] corroborates the idea that thermal activation is indeed more pronounced in nanostructures than in continuous FM-AFM bilayers. The derivatives dH_E/dT_{heat2}, which are plotted in Fig. 3(b) are typically used to represent the blocking temperature distribution of FM-AFM bilayers.[1] As can be seen in the figure, these T_B distributions are overall shifted towards lower temperature values for the nanostructures. It can be argued that, due to their reduced coordination numbers, AFM spins located at the edges of the dots can be more easily dragged during the magnetization reversal of the FM, which might account for the weakening of the pinning strength and the enhanced thermal activation in the nanostructures. This can bring about an enhancement of H_C in the nanostructures, which is also observed in our case (see Fig. 2).

Figure 3(a) shows as well that, for both continuous films and nanostructures, thin AFM layers are more clearly affected by thermal activation effects than thicker ones, since H_E decreases faster with T_{heat2} for thinner AFM layers. This

is in agreement with the often reported reduction of T_B for low values of t_{AFM}.[1,14,23,27,33] This also manifests in a shift towards higher values of the blocking temperature distribution for thicker AFM layers, as can be seen in Fig. 3(b). It should be noted that a coherent columnar growth of the layers could be assessed from x-ray diffraction measurements. Namely, the vertical coherence lengths extracted from the widths of θ-2θ scan peaks showed that a good structural coherence exists within each grain throughout the AFM. As a result, for thicker AFM, the grains are expected to maintain the AFM order up to larger values of temperature.[1] Note that the T_B distributions also seem to slightly broaden for thicker AFM. The fact that for thicker IrMn layers thermal activation effects may be important over a slightly broader range of temperatures could be due to an increasing number of defects in the AFM layer, or to a broadening in the grain size distribution.

Figure 4 shows the evolution of H_E, estimated from the hysteresis loops measured at room temperature, on t_{IrMn} for both the continuous films and the nanostructures, after the first field cooling process using a positive field from T_{heat1} =550 K [shown in Fig. 4(a), taken from Fig. 2 of Ref. 23] and after the subsequent field cooling under a negative field, from T_{heat2}=313, 333, and 353 K [shown in Figs. 4(b)–4(d), respectively]. After the first field cooling procedure, H_E in the continuous films decreases as t_{IrMn} increases whereas H_E in the nanostructures seems to be rather insensitive to t_{IrMn}. As a result, although H_E in the nanostructures is smaller than for the continuous films for thin AFM layers, larger H_E in the dots is observed for t_{IrMn} larger than 12 nm.[23] These behaviors can be ascribed to the three-dimensional confinement of AFM domains in the nanostructures. Namely, the decrease of H_E with the AFM thickness is often observed in continuous FM-AFM systems[1,23,25,28,31] and can be attributed to the increase of the AFM domain size with the AFM thickness. Such inverse proportionality relationship between H_E and the AFM thickness was already predicted by Malozemoff in his random field model for exchange bias, in the so-called Heisenberg regime[3] and has been proved to be valid also in the framework of the so-called domain state model.[31] According to Malozemoff's model, in a given interface area L^2 (which would correspond to the characteristic AFM domain size), containing N atoms (so that $N=L^2/a^2$, where a is the lattice constant), the local FM-AFM interface energy $\sigma_l = \pm J/a^2$ (whose sign depends on the local orientation between the FM and AFM spins) averages statistically as $\sigma = \sigma_l/N^{1/2}$ (thus being inversely proportional to L, the AFM domain size). For IrMn, using appropriate values of anisotropy and exchange constants, the domain size can be estimated to range between 160 nm for t_{IrMn}=5 nm and 620 nm for t_{IrMn}=19 nm.[23] Hence, although the AFM domain size increases with t_{IrMn} for the continuous films, resulting in a reduction of H_E, its evolution is physically limited by the dots sizes (i.e., 90 nm) in the nanostructures, thus maintaining a constant value of H_E in the overall t_{IrMn} range. As a result of the enhanced thermal activation in thin and/or nanostructured AFM, the reduction of H_E with t_{IrMn} is smoothed for the continuous films as T_{heat2} increases,[11] and, in contrast, H_E starts to increase with t_{IrMn} for the nanostructures. It is noteworthy that assuming that AFM spins are more easily unpinned due to thermal activation for thinner AFM layers, one might expect H_E to increase with t_{IrMn} in the nanostructures, even at room temperature. This is not observed probably because room temperature is still rather low compared with the maximum blocking temperature for these compositions (e.g., $T_B \sim 390$ K for t_{IrMn}=5 nm in the nanostructures[23]).

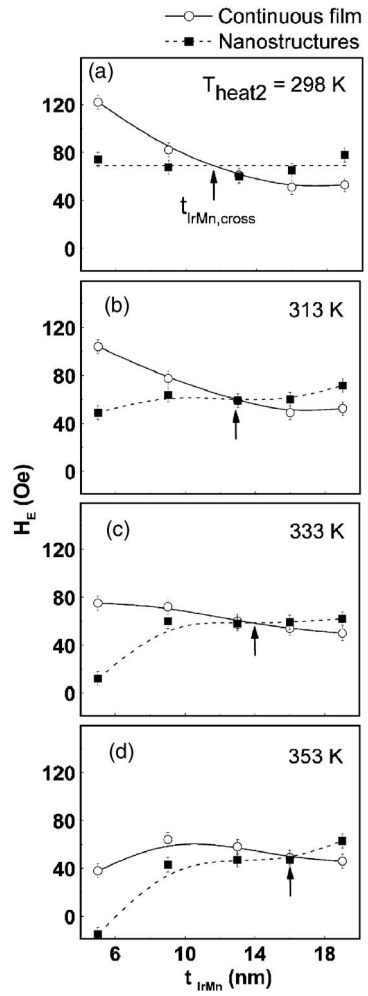

FIG. 4. Dependence of the exchange bias field H_E on the IrMn thickness t_{IrMn} for both continuous films (-○-) and nanostructures (-■-) with compositions Ta(5 nm)/Py(12 nm)/IrMn(t_{IrMn})/Pt(2 nm), (a) after a first field cooling (H_{FC}=2.4 kOe) from 550 K and (b)–(d) after a second field cooling (H_{FC}=−2.4 kOe) from different heating temperatures (T_{heat2}=313, 333, and 353 K). The lines are guides to the eye. The arrows show the intersection of the evolutions in the nanostructures and in the continuous film. Note that Fig. 4(a) has been taken from Fig. 2 of Ref. 23.

As can be seen in Fig. 4 the value of t_{IrMn} at which, for a given T_{heat2}, the evolutions of H_E on t_{IrMn} for the nanostructures and the continuous film intersect, $t_{IrMn,cross}$ increases with T_{heat2}. This means that for lower heating temperatures the exchange bias in the nanostructures is found to be larger than for the continuous films in a broader AFM thickness range. It should be noted that, due to thermal activation, even at heating temperatures larger than room temperature, thicker layers are required to obtain larger H_E in the nanostructures than in continuous films.

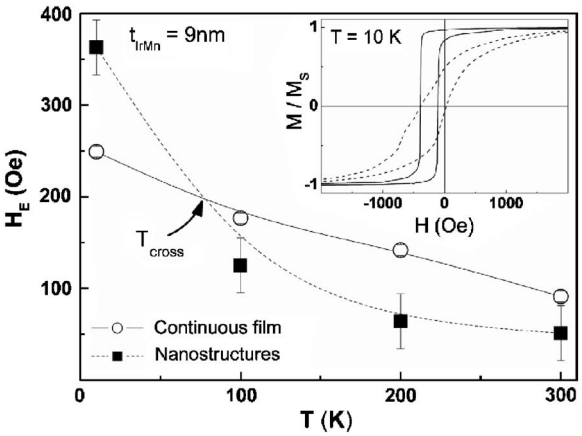

FIG. 5. Dependence of the exchange bias field H_E on the temperature T for both the continuous films (-○-) and the nanostructures (-■-), with compositions Ta(5 nm)/Py(12 nm)/IrMn(9 nm)/Pt(2 nm). The lines are guides to the eye. The inset shows the corresponding hysteresis loops measured at 10 K by SQUID along the field cooling direction, after cooling from T=550 K in the presence of a 2.4 kOe field.

Figure 5 shows the evolution of H_E on the temperature T for low temperatures ranging from 10 to 300 K, deduced from hysteresis loops measured by SQUID (a typical one is shown in the inset for T=10 K), for both continuous film and nanostructures with composition Ta(5 nm)/Py(12 nm)/IrMn(9 nm)/Pt(2 nm). In contrast to longitudinal Kerr effect measurements, SQUID magnetometry measurements probe both the signal from the dots and that from the trenches, i.e., from material deposited between the dots. However, the two magnetic contributions are well enough separated, hence making it possible to roughly estimate the exchange bias from the nanostructures. The loop corresponding to the patterned array (inset of Fig. 5) shows that the ascending branches of the dots and the trenches virtually match. On the contrary, the descending branch clearly exhibits two steps. The larger step (about 3/4 of the signal, in agreement with the expected signals ratio) corresponds to the signal from the trenches, and the smaller step, at higher negative fields corresponds to the signal from the dots, which is the signal of interest here. It is noteworthy that, at 10 K, for t_{IrMn}=9 nm, the hysteresis loop of the continuous film is shifted towards lower values than the hysteresis loop of the dots, in contrast to the behavior reported in Fig. 5, and in Fig. 4(a) for higher temperatures.

As already discussed, the decrease of H_E with T for both the continuous film and the nanostructures shown in Fig. 5 can be ascribed to thermally induced weakening of AFM spins pinning strength when T increases, effect which is still visible at lower sweep field rate with comparison to the sweep field rate used for MOKE measurements. The fact that H_E decreases faster in the nanostructures confirms that nanostructured AFM layers are more subject to thermal activation effects than continuous films. This is in agreement with some results reported in the literature on low-temperature measurements of FM-AFM exchange biased nanostructures, which also show that H_E decreases faster as T is increased for confined AFM layers than for continuous films.[11] It is remarkable that, when thermal activation effects are minimized, the nanostructures with thin AFM layers can exhibit larger exchange bias than the continuous films, as it occurs at high temperatures for the nanostructures with thicker AFM layers (see in Fig. 4). This is in agreement with Malozemoff's static model predictions, which neglects the influence of thermal activation and predicts larger exchange bias for smaller AFM domain size.[4]

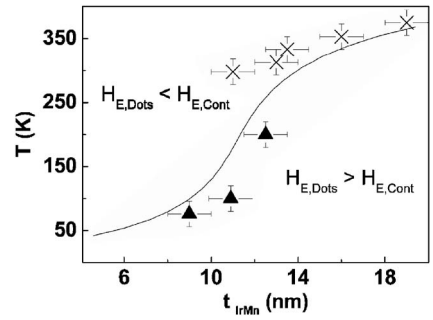

FIG. 6. Phase diagram showing the temperature T and IrMn thickness t_{IrMn} conditions for which the exchange bias field of sub-100 nm nanostructures ($H_{E,dots}$) is either larger or smaller than that of continuous films ($H_{E,cont}$) with the same composition, at the same temperature. Note that the (-x-) data is deduced from room temperature Kerr effect measurements after the cooling in negative field from T_{heat2}, whereas the (-▲-) data is deduced from low-temperature SQUID measurements. The line is a guide to the eye.

From the evolutions of H_E on T and t_{IrMn}, it is possible to extract the conditions for which H_E in the dots, $H_{E,dots}$ is larger or smaller than H_E in the continuous films $H_{E,cont}$. This is shown in Fig. 6. The data plotted in the figure have been deduced from the evolutions of H_E on T_{heat2} and t_{IrMn} (i.e., Fig. 4), from low-temperature evolutions of H_E on t_{IrMn}, and from low-temperature evolutions of H_E on T (Fig. 5). For instance, from Fig. 4, the value of t_{IrMn} at which the evolutions of H_E on t_{IrMn} for the nanostructures and the continuous film cross ($t_{IrMn,cross}$) for a given T_{heat2}, shows the transition from $H_{E,dots} > H_{E,cont}$ to $H_{E,dots} < H_{E,cont}$, and is then plotted in Fig. 6. Similarly, from Fig. 5, the value of T at which the evolutions of H_E on T for the nanostructures and the continuous film intersect is also plotted in Fig. 6. This allows depicting a phase diagram, which summarizes the trends discussed above and can be understood with having in mind that the AFM spin structure is more prone to thermal activation for thin AFM layers and for the nanostructures. Note however that different field sweep rates were used for SQUID (about 0.03 Oe s^{-1}) and MOKE (about 1 Oe s^{-1}) measurements. Since thermal activation effects are more effective for the nanostructures, one would expect that H_E decreases slightly faster with the field sweep rate for the nanostructures with respect to the continuous film, resulting in a slight overestimation of T_{cross} as determined from SQUID measurements (see Fig. 5), i.e., at low field sweep rate, compared to that which would be measured using a higher rate, by MOKE.

Note that the magnetostatic energy of the FM layer in patterned EB bilayers might change the FM domain wall density during the reversal of the FM layer thus influencing H_C and H_E.[19–22,40] The small size of the dots (90 nm) did not

allow us to determine by MFM the exact reversal process of the FM. However, from the hysteresis loops, it is very likely that the reversal occurs via coherent rotation of the FM, or via the formation of high remanence states, but not via the formation of vortex or pronounced low remanence states.[19–22] It has been theoretically shown that for 100 nm lateral dot size and $t_{Py}=10$ nm, in the case of high remanence configurations, magnetostatic interactions can enhance H_E by 10% for the nanostructures with respect to continuous films.[40] It is thus not to be excluded that magnetostatic interactions contribute to the H_E enhancement in the nanostructures. Note, however, that some AFM spins are certainly dragged during the magnetic reversal of the FM layer. Remark as well that at low temperatures (see Fig. 5), when thermal activation effects, which tend to reduce H_E in the nanostructures are minimized, H_E in the nanostructures is enhanced by more than 40%. It is thus very likely that other effects such as, for example, AFM domain constraints previously discussed, contribute, to a large extent, to the enhancement of H_E in the nanostructures.

It is noteworthy that our results might shed light on some of the opposite behaviors reported in the literature. For example, Ref. 8 reports an enhancement of H_E in nanostructured CoO whereas Ref. 18 shows the opposite behaviour. Indeed, this might be ascribed to both the use of thicker CoO layer (10 nm) and higher temperature (77 K) in Ref. 8 than in Ref. 18 (3 nm, 5 K). Similarly, for NiO,[10–12] a reduction of H_E, in the nanostructures with respect to continuous films, is observed for thin AFM layers[12] and an enhancement is observed for thicker AFM layers.[10,11] Likewise our results on thermal activation in exchange biased nanostructures are consistent with previous works, and might thus contribute to better understand some of the reported temperature dependant evolution of H_E in nanostructures, such as, for example, Refs. 11 and 12.

IV. CONCLUSION

In conclusion, pronounced thermal activation effects have been observed in sub-100 nm Py/IrMn nanostructures compared with continuous films with the same composition. In addition, thinner AFM layers are found to be more prone to thermal activation. These results are ascribed to the spatial constraints imposed on the formation of AFM domains, which probably result in a loosely pinned AFM spin structure. As a result of the interplay between thermal activation effects, favoring a reduction of H_E in the nanostructures, and the AFM domain size reduction imposed by the reduced lateral dimensions of the nanostructures, which favor the opposite behavior, the hysteresis loop shift for the nanostructures can be either *larger* or *smaller* than that of continuous films with the same composition, depending on both the AFM layer thickness and temperature conditions.

ACKNOWLEDGMENTS

This work was supported by the European Community through the NEXBIAS Grant No. HPRN-CT-2002-00296. The authors acknowledge S. Auffret and J.-F. Jacquot for their technical assistance. We are also grateful to J. Nogués for the critical reading of the manuscript and the concomitant fruitful discussions.

*Electronic mail: baltz@drfmc.ceng.cea.fr

[1] For recent reviews on exchange bias, see J. Nogués and I. K. Schuller, J. Magn. Magn. Mater. **192**, 203 (1999); A. E. Berkowitz and K. Takano, *ibid.* **200**, 552 (1999); R. L. Stamps, J. Phys. D **33**, R247 (2000); M. Kiwi, J. Magn. Magn. Mater. **234**, 584 (2001).
[2] D. Mauri, H. C. Siegmann, P. S. Bagus, and E. Kay, J. Appl. Phys. **62**, 3047 (1987).
[3] A. P. Malozemoff, Phys. Rev. B **35**, R3679 (1987); **37**, 7673 (1988).
[4] A. Scholl, F. Nolting, J. W. Seo, H. Ohldag, J. Stöhr, S. Raoux, J.-P. Locquet, and J. Fompeyrine, Appl. Phys. Lett. **85**, 4085 (2004).
[5] H. Ohldag, A. Scholl, F. Nolting, E. Arenholz, S. Maat, A. T. Young, M. Carey, and J. Stöhr, Phys. Rev. Lett. **91**, 017203 (2003).
[6] B. Dieny, V. S. Speriosu, S. S. P. Parkin, B. A. Gurney, D. R. Wilhoit, and D. Mauri, Phys. Rev. B **43**, 1297 (1991).
[7] S. Tehrani, J. M. Slaughter, M. Deherrera, B. N. Engel, N. D. Rizzo, J. Slater, M. Durlam, R. W. Dave, J. Janesky, B. Butcher, K. Smith, and G. Grynkewich, Proc. IEEE **91**, 703 (2003).
[8] T. Kimura, G. Mozumi, F. Wakaya, and K. Gamo, Jpn. J. Appl. Phys., Part 1 **40**, 2241 (2001).
[9] K. Liu, S. M. Baker, M. Tuominen, T. P. Russell, and I. K. Schuller, Phys. Rev. B **63**, 060403(R) (2001).
[10] J. C. Wu, H. W. Huang, C. H. Lai, and T. H. Wu, J. Appl. Phys. **87**, 4948 (2000).
[11] A. Nemoto, Y. Otani, S. G. Kim, K. Fukamichi, O. Kitakami, and Y. Shimada, Appl. Phys. Lett. **74**, 4026 (1999).
[12] M. Fraune, U. Rüdiger, G. Güntherodt, S. Cardoso, and P. Freitas, Appl. Phys. Lett. **77**, 3815 (2000).
[13] J. Sort, H. Glaczynska, U. Ebels, B. Dieny, M. Giersig, and J. Rybczynski, J. Appl. Phys. **95**, 7516 (2004).
[14] V. Baltz, J. Sort, B. Rodmacq, B. Dieny, and S. Landis, Appl. Phys. Lett. **84**, 4923 (2004).
[15] J. Yu, A. D. Kent, and S. S. P. Parkin, J. Appl. Phys. **87**, 5049 (2000).
[16] Y. Shen, Y. Wu, H. Xie, K. Li, J. Qiu, and Z. Guo, J. Appl. Phys. **91**, 8001 (2002).
[17] Z. B. Guo, K. B. Li, G. C. Han, Z. Y. Liu, P. Luo, and Y. H. Wu, J. Magn. Magn. Mater. **251**, 323 (2002).
[18] E. Girgis, R. D. Portugal, H. Loosvelt, M. J. Van Bael, I. Gordon, M. Malfait, K. Temst, C. Van Haesendonck, L. H. A. Leunissen, and R. Jonckheere, Phys. Rev. Lett. **91**, 187202 (2003).
[19] J. Eisenmenger, Z.-P. Li, W. A. A. Macedo, and I. K. Schuller, Phys. Rev. Lett. **94**, 057203 (2005).
[20] Z.-P. Li, O. Petracic, J. Eisenmenger, and I. K. Schuller, Appl. Phys. Lett. **86**, 072501 (2005).

[21] J. Sort, A. Hoffmann, S. H. Chung, K. Buchanan, V. Novosad, M. Grimsditch, M. D. Baró, B. Dieny, and J. Nogués (unpublished).
[22] A. Hoffmann, M. Grimsditch, J. E. Pearson, J. Nogués, W. A. A. Macedo, and I. K. Schuller, Phys. Rev. B **67**, 220406(R) (2003).
[23] V. Baltz, J. Sort, S. Landis, B. Rodmacq, and B. Dieny, Phys. Rev. Lett. **94**, 117201 (2005).
[24] T. Eimüller, T. Kato, T. Mitzuno, S. Tsunashima, C. Quitmann, T. Ramsvik, S. Iwata, and G. Schütz, Appl. Phys. Lett. **85**, 2310 (2004).
[25] T. Ambrose and C. L. Chien, J. Appl. Phys. **83**, 6822 (1998).
[26] W. Pan, N.-Y. Jih, C.-C. Kuo, and M.-T. Lin, Appl. Phys. Lett. **95**, 7297 (2004).
[27] J. P. Nozières, S. Jaren, Y. B. Zhang, A. Zeltser, K. Pentek, and V. S. Speriosu, J. Appl. Phys. **87**, 3920 (2000).
[28] T. Hughes, K. O'Grady, H. Laidler, and R. W. Chantrell, J. Magn. Magn. Mater. **235**, 329 (2001).
[29] A. Hoffmann, Phys. Rev. Lett. **93**, 097203 (2004).
[30] S. Soeya, S. Nakamura, T. Imagawa, and S. Narishige, J. Appl. Phys. **77**, 5838 (1995); S. Soeya, T. Himagawa, K. Mitsuoka, and S. Narishige, *ibid.* **76**, 5356 (1994).
[31] M. Ali, C. H. Marrows, M. Al-Jawad, B. J. Hickey, A. Misra, U. Nowak, and K. D. Usabel, Phys. Rev. B **68**, 214420 (2003).
[32] E. Fulcomer and S. H. Charap, J. Appl. Phys. **43**, 4184 (1972); **43**, 4190 (1972).
[33] H. Xi, J. Magn. Magn. Mater. **288**, 66 (2005).
[34] M. D. Stiles and R. D. McMichael, Phys. Rev. B **60**, 12 950 (1999).
[35] R. L. Stamps and L. Wee, IEEE Trans. Magn. **36**, 3170 (2000).
[36] S. Landis, B. Rodmacq, and B. Dieny, Phys. Rev. B **62**, 12 271 (2000).
[37] J. I. Martin, J. Nogués, K. Liu, J. L. Vicent, and I. K. Schuller, J. Magn. Magn. Mater. **256**, 449 (2003).
[38] R. Skomski, J. Phys.: Condens. Matter **15**, R841 (2003).
[39] C. Leighton, M. R. Fitzsimmons, A. Hoffmann, J. Dura, C. F. Majkrzak, M. S. Lund, and I. K. Schuller, Phys. Rev. B **65**, 064403 (2002).
[40] S. Zhang and Z. Li, Phys. Rev. B **65**, 054406 (2001).